



## Relaxation behavior of supra-molecular hydrogen-bonded liquid crystal phase structures: SA:11OBA

A. V. N. Ashok Kumar, M. Muniprasad, A. V. S. N. Krishna Murthy, P. V. Chalapathi & D. M. Potukuchi

To cite this article: A. V. N. Ashok Kumar, M. Muniprasad, A. V. S. N. Krishna Murthy, P. V. Chalapathi & D. M. Potukuchi (2016) Relaxation behavior of supra-molecular hydrogen-bonded liquid crystal phase structures: SA:11OBA, *Molecular Crystals and Liquid Crystals*, 624:1, 28-43, DOI: [10.1080/15421406.2015.1038884](https://doi.org/10.1080/15421406.2015.1038884)

To link to this article: <http://dx.doi.org/10.1080/15421406.2015.1038884>



Published online: 11 Feb 2016.



Submit your article to this journal [↗](#)



Article views: 78



View related articles [↗](#)



View Crossmark data [↗](#)

## Relaxation behavior of supra-molecular hydrogen-bonded liquid crystal phase structures: SA:11OBA

A. V. N. Ashok Kumar<sup>a</sup>, M. Muniprasad<sup>a</sup>, A. V. S. N. Krishna Murthy<sup>a</sup>, P. V. Chalapathi<sup>b</sup>, and D. M. Potukuchi<sup>a</sup>

<sup>a</sup>Department of Physics, University College of Engineering, Jawaharlal Nehru Technological University, Kakinada, Andhra Pradesh, India; <sup>b</sup>Department of Physics, University of Gondar, College of Natural and Computational Sciences, Ethiopia

### ABSTRACT


Low-frequency (20 Hz–10 MHz) dielectric response in liquid crystalline (LC) phases of hydrogen-bonded (HB) complex, SA:11OBA, is studied. Synthesis of SA:11OBA with non-mesogenic succinic acid (SA) and mesogenic p-n-undecyloxy benzoic acid (11OBA) and its spectroscopic confirmation are detailed. Phase transition temperatures ( $T_c$ ) involving nematic, smectic-C (SmC), and smectic-G (SmG) phases by capacitance  $C(T)$  and loss  $\tan\Delta(T)$  anomaly agree with the microscopy (polarizing optical microscope) and calorimetry (differential scanning calorimetry) results. Low-frequency dispersion infers two types of reorientation processes, viz. higher frequency ( $\sim$ MHz) and lower frequency (kHz) processes. Distinct time scale mechanism are presented. Arrhenius behavior infers influence of HB on activation energy ( $E_a$ ). Off-centered dispersion, viz.  $\varepsilon'(\omega)$  with  $\varepsilon''(\omega)$ , analyzed through the Cole–Cole plots in N, SmC, and SmG phases infers a strong temperature trend for dielectric strength ( $\Delta\varepsilon$ ) and distribution ( $\alpha$ ) parameters. Temperature dependence of  $\alpha$ -parameter reveals on LC phases increasing fixture of molecular dipole in LC phase structure. Results are discussed in the wake of the body of data reported in LC phases exhibited by other LC compounds.

### KEYWORDS

Hydrogen Bonding; InfraRed Spectra; Differential Scanning Calorimetry; Low-Frequency Dielectric Dispersion; Activation Energy; Relaxation Behavior

## 1. Introduction

Liquid crystal (LC) materials belong to an interesting family of soft matter due to their excelling [1–3] electro-optic (EO) performance. The fundamental aspect [4, 5] of exotic symmetries that tune thermodynamic parameters across LC phase transitions is interesting. Nevertheless, the information of integrated response of LC phase structure to the applied field provides an equivalently interesting data base for their utility in devices. Response [2, 5] of an LC phase structure is mapped to external stimulus through the details of underlying microscopic interactions. Thus, the utility of an LC phase in an EO device owes to the optimization of their dielectric response and relaxation behavior. Each of the LC phase structure is characteristically constituted by a stable assembly of molecular dipoles. The data [6–10] regarding the field and temperature dependence of anisotropic dipolar response, collective excitations,

**CONTACT** D. M. Potukuchi ✉ [dakshinamurthy\\_potukuchi@yahoo.com](mailto:dakshinamurthy_potukuchi@yahoo.com)  Department of Physics, University College of Engineering, Jawaharlal Nehru Technological University, Kakinada 533003, Andhra Pradesh, India.

Color versions of one or more of the figures in the article can be found online at [www.tandfonline.com/gmcl](http://www.tandfonline.com/gmcl).

© 2016 Taylor & Francis Group, LLC

relaxation mechanism ( $f_R$ ), dielectric strength ( $\Delta\epsilon$ ), distribution parameter ( $\alpha$ ), and molecular dynamics at LC interfaces have represented a powerful tool in harnessing LC systems.

The LC phase structure represents the fourth state of matter. Its growth with temperature is tuned by diversified interactions among molecular dipoles. Thus, growth of LC phase finally manifests as the observed anisotropic response. Although Debye's theory [11] of dielectric relaxation relies on point dipole concept, the evolutionary [6] changes that are witnessed in the area of real molecular LC systems adopted the resolved anisotropic dipole concept. In this direction, the Cole–Davidson theory [10] as adopted by Kresse and Moscicki [12] addressed the topic of off-centered dielectric dispersion exhibited by LC phase structures with a possible utility of corresponding dielectric modes in EO displays.

Nematic phases that are widely used in LC displays [13] are initially identified to operate at a millisecond speed. Subsequently, research reported [14] in LCs in their chiral tilted phases (or smectic-C\* (SmC\*)) has witnessed a rather fast switching response in sub-microsecond range in their surface stabilized geometry (SSFELC). Further, during their effort to realize the tilted LC SmC phase structures at operationally viable ambient temperatures, researchers opted to follow the route of supra molecular (SM) design [15–22] of LCs. However, the field area of SMLCs seems to be dominated [23, 24] by the majority of LC reports involving hydrogen-bonded (soft covalent or HB) interaction. Hence, the research in the Hydrogen-Bonded Liquid Crystals (HBLCs) heralded a new era. The advantage [25–37] with the HBLCs of calamitic-type vouched for the extended LC phase stability, and enhanced the diversity of tilted phases, induction tilted phases, and shifted thermal stability toward room temperature (RT).

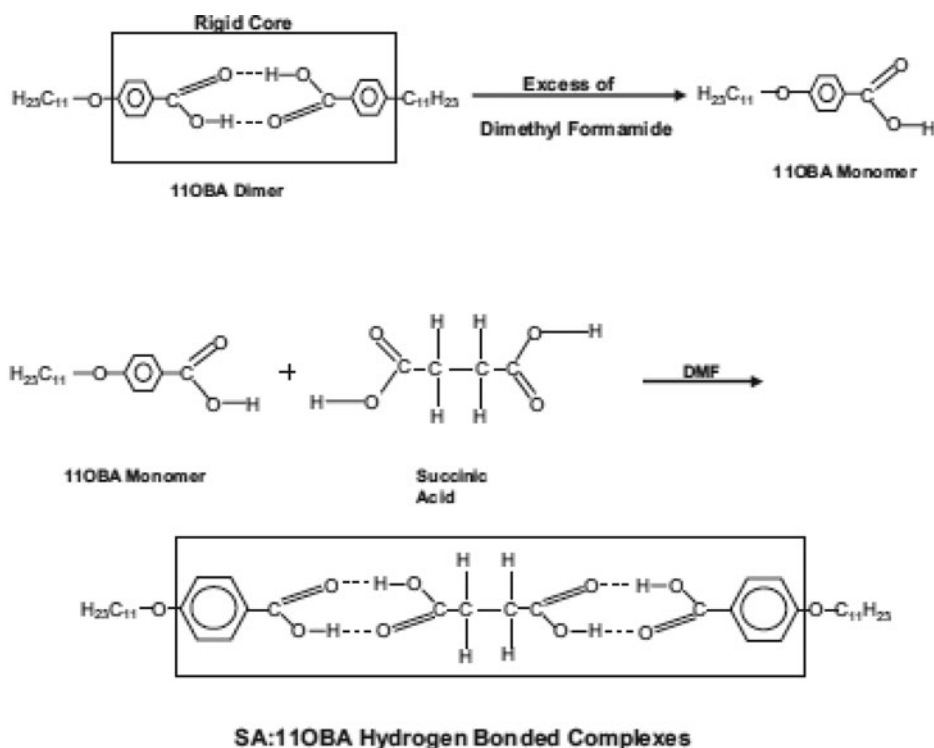
Low frequency (LF) dielectric response in nematic (N) phase structure is extensively reported [38–42] in literature along with its relaxation behavior. LF dielectric investigations are also reported [7, 12, 43] in calamitic LCs regarding their collective response and the influence of field in different modes in SmC\* phases with chiral center. However, LF dielectric response is scantily reported [43] in calamitic LCs that possess HB interaction. The higher homologues of calamitic LC series possessing HB interaction are reported [25–37, 44] to exhibit enhanced device savvy tilted polymorphism. In the wake of importance of tilted LC phases, authors presented the investigations of the LF dielectric (20 Hz to 10 MHz) response in an HBLC complex, viz., SA:11OBA [45] nematic, SmC and SmG phases.

The paper is organized in three sections. Introduction to LF dielectric relaxation studies in LC phases and device savvy nature of HBLCs are presented in Section 1. Details of synthesis, confirmation of the product, and methods experimental of characterization are described in Section 2. The experimental results are presented and discussed along with relevant interpretation in Section 3.

## 2. Experimental

### 2.1. Synthesis of SA:11OBA Hydrogen-Bonded LC complex

The HBLC complex, SA:11OBA, is synthesized by following the procedure reported earlier for lower homologues [46]. HBLC complex is synthesized by adding two moles of p-n-undecyloxy benzoic acid, i.e., 11OBA with one mole of succinic acid (SA) in N,N-dimethyl formamide (DMF). Further, it is subjected to constant stirring for 10 hrs at ambient temperature (30°C) till a white precipitate is formed. The white crystalline crude complex is obtained by removing excess DMF. The product is then re-crystallized with dimethyl sulphoxide (DMSO). The yield of the reaction for SA:11OBA is observed to be ~70%. The synthetic



**Scheme 1.** Scheme of synthesis for preparation of SA:11OBA.

route and the proposed molecular structure for the present HBLC complex, viz. SA:11OBA is presented as end product in [Scheme 1](#). The compound SA:11OBA so isolated is visually observed as a white crystalline solid. It is found to be stable at room temperature. The HBLC complex is found to melt around a temperature of  $\sim 72^\circ\text{C}$ . It is found to exhibit high thermal and chemical stability.

## 2.2. Methods and materials

Chemical ingredients, viz. nOBAs (for  $n = 11$ ) succinic acid(SA), and solvents, viz. tetrahydrofuran (THF), DMSO, deuterated chloroform ( $\text{CDCl}_3$ ), and tetramethyl silane,  $\text{Si}(\text{CH}_3)_4$ , are procured from Sigma Aldrich USA. The confirmation of molecular formula (i.e. abundance of H-atoms), formation of HB, and purity of LC complexes are confirmed [47, 48] by  $^1\text{H}$  Nuclear Magnetic Resonance (NMR) (Avance, 300 MHz) and infrared (IR) (Schimadzu-8701 FTIR) spectroscopy. An SD-Tech. polarizing optical microscope (POM) equipped with a  $\mu$ -master digital CCD camera in conjunction with Photo-Manager (OEM) software is used. An Instec HCS-402 heating stage and STC-200 temperature controller (with a resolution of  $\pm 0.1^\circ\text{C}$ ) are used to determine the LC phase transition temperatures ( $T_C$ ). Microscopic slides for POM textural studies are carried out with the help of glass plate-cum-cover-slip combination. Unidirectional rubbing (with filter paper) is carried out on glass plate to promote homogenous alignment of samples. Homogeneously aligned LC samples (for POM) are prepared by introducing samples in  $5\text{-}\mu\text{m}$  spaced (Device Tech. USA) pre-treated cells by capillary action (in isotropic liquid state). LC phases, transition temperatures ( $T_C$ ), and enthalpy ( $\Delta H$ ) values are determined (a resolution of  $\pm 0.1^\circ\text{C}$ ) with the help of a Schimadzu DSC-60 system, operated at a heating/cooling rate of  $10^\circ\text{C}/\text{min}$ .

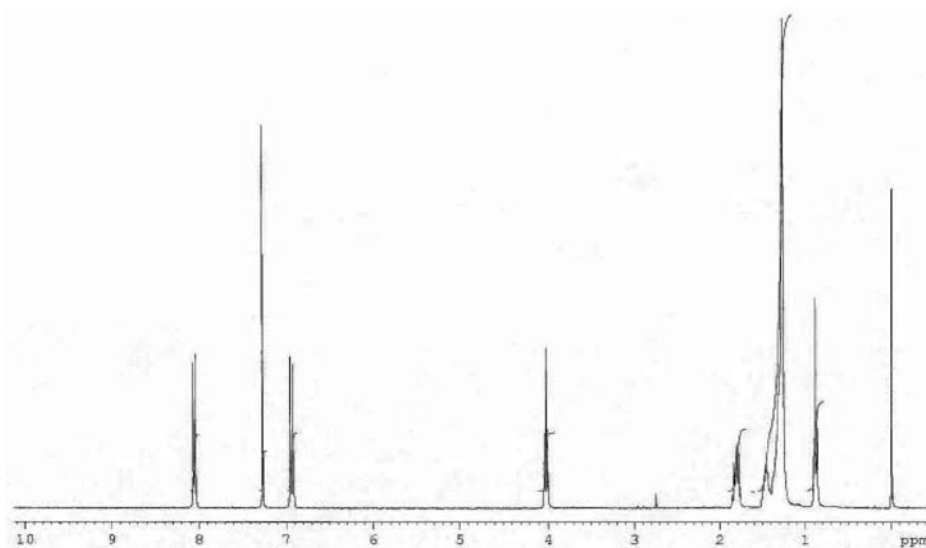


**Figure 1.**  $^1\text{H}$  NMR spectra of SA:11OBA complex.

### 3. Results and discussion

#### 3.1. $^1\text{H}$ NMR study for SA:11OBA HBLC complex

The  $^1\text{H}$  NMR spectra corresponding to SA:11OBA complex is given in Fig. 1. The salient features of the spectra are as follows:

1. A triplet at  $\delta$  0.88 ppm ( $J = 6.632$  Hz) confirms the presence of methyl groups at both ends of the complex.
2. A set of multiplets in the range of  $\delta$  1.27–1.48 ppm infers the presence of methylene groups.
3. Multiplet at the vicinity of  $\delta$  1.76–1.83 ppm corresponds to  $\text{CH}_2\text{CO}$  groups of succinic acid.
4. Existence of a triplet at  $\delta$  1.76 ppm ( $J = 6.55$  Hz) indicates the presence of  $\text{ArOCH}_2$  group of *n*-alkoxy benzoic acid.
5. Doublets at  $\delta$  6.93 ppm ( $J = 8.9139$  Hz) and  $\delta$  8.04 ppm ( $J = 8.88$  Hz) show the presence of aromatic proton.
6. A singlet peak at  $\delta$  7.26 ppm is due to residual protons of  $\text{CDCl}_3$ , which is used as a solvent.

**Details of the spectra.**  $\delta$  0.88 ppm (t,  $J = 6.63$  Hz, 6H,  $2\text{X CH}_3$ ),  $\delta$  1.27–1.48 ppm (m,  $-\text{CH}_2-$ ),  $\delta$  1.76–1.83 ppm (m, 4 H,  $-\text{CH}_2\text{CO}-$ ),  $\delta$  4.022 ppm (t,  $J = 6.55$  Hz, 4 H,  $\text{ArOCH}_2$ ),  $\delta$  6.93 ppm (d,  $J = 8.91$  Hz, 4H, Ar-H),  $\delta$  8.04 ppm (d,  $J = 8.88$  Hz, 4H, Ar-H).

Since the observed  $^1\text{H}$  NMR spectra agree with the expected protonic abundance of targeted complex [46] (Scheme 1), the synthesis is confirmed successful. The product SA:11OBA is confirmed for its purity at spectroscopic level.

#### 3.2. IR study of SA:11OBA HBLC complex

The room temperature solid state (KBr) IR spectrum of SA:11OBA is presented in Fig. 2 along with that of pure 11OBA in Fig. 3. The important features of the spectrum are as follows:

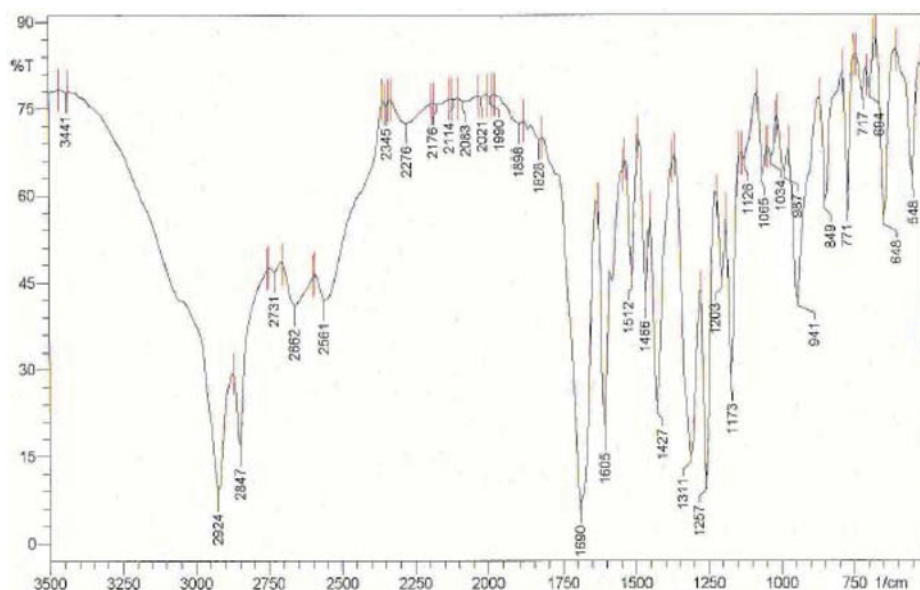


**Figure 2.** IR spectra of SA:11OBA complex.

1. The disappearance of double peak at  $\sim 1700\text{ cm}^{-1}$  pertaining to carbonyl group of nOBAs and appearance of single peak at  $1690\text{ cm}^{-1}$  imply a bathochromic shift by  $10\text{ cm}^{-1}$ . This observation proves a clinching evidence for the participation of acid moiety ( $-\text{COOH}$ ) of nOBA in the formation of HB complex.
2. The existence of a strong absorption band at  $2924\text{ cm}^{-1}$  indicates the shift of hydroxyl ( $-\text{OH}$ ) stretching frequency of acid ( $-\text{COOH}$ ) group of nOBA by  $84\text{ cm}^{-1}$ . This shift confirms the participation of  $-\text{OH}$  group of nOBA in HB formation with SA.
3. The stretching absorption for carbonyl group of succinic acid (aliphatic acid) is noted to be shifted to  $1728\text{ cm}^{-1}$  instead of its expected appearance at  $\sim 1700\text{ cm}^{-1}$ . This shift also provides substantial evidence for the participation of  $-\text{OH}$  group of SA in HB formation with nOBAs.

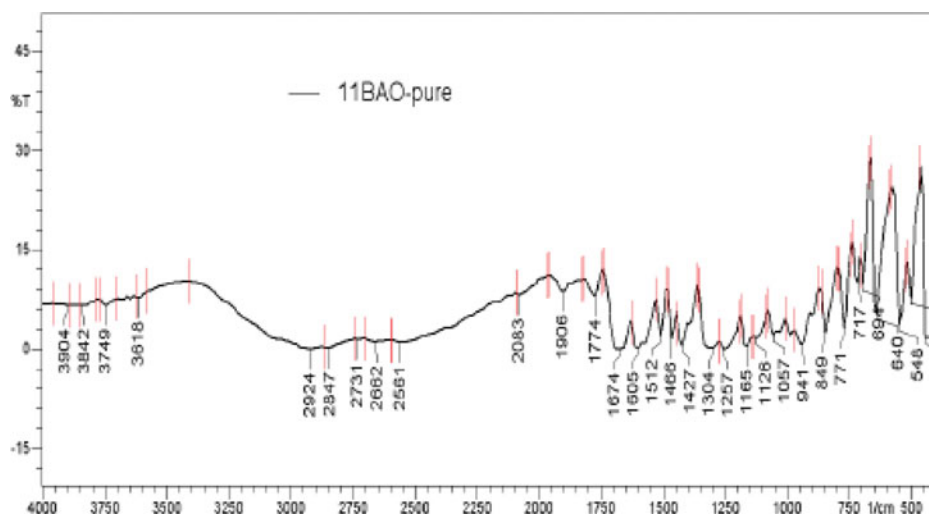


**Figure 3.** IR spectra of 11OBA complex.



4. The IR absorption pertaining to  $\text{-OH}$  group of SA, which is expected at  $>3600\text{ cm}^{-1}$ , is found to be shifted to  $3448\text{ cm}^{-1}$ . Such a bathochromic shift confirms the involvement of  $\text{-OH}$  group of  $\text{-COOH}$  moiety in SA in forming of hydrogen bond during complexation.

In view of the cited features [46] and the observations in Figs. 2 and 3 of IR spectra, the formation of HB between the SA and 11OBA moieties is confirmed. As such, the case of HB in SA:11OBA is confirmed as inter-molecular, linear, and complementary-type of bond formed between non-mesogenic (SA) and mesogenic (nOBA) moieties as proposed in Scheme 1.

### 3.3. Polarized optical microscopy (POM)

Textures exhibited by SA:11OBA at different temperatures during heating and cooling scans are recorded. Any observed change in texture at a temperature is identified as phase transition temperature  $T_C$ . The characteristic textures [49] are found to be exhibited by SA:11OBA. Nematic phase exhibits (Plate 1) the Schleiren-threaded texture, SmC phase exhibits (Plate 2)

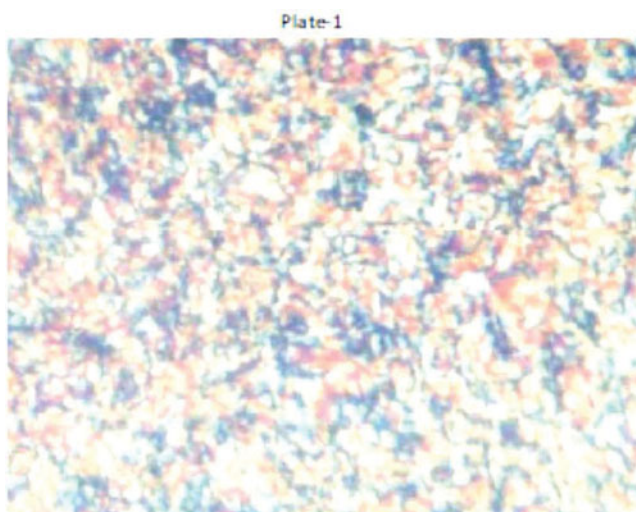


**Plate 1.** Schleiren-threaded texture of nematic phase for SA:11OBA at  $133^\circ\text{C}$ .

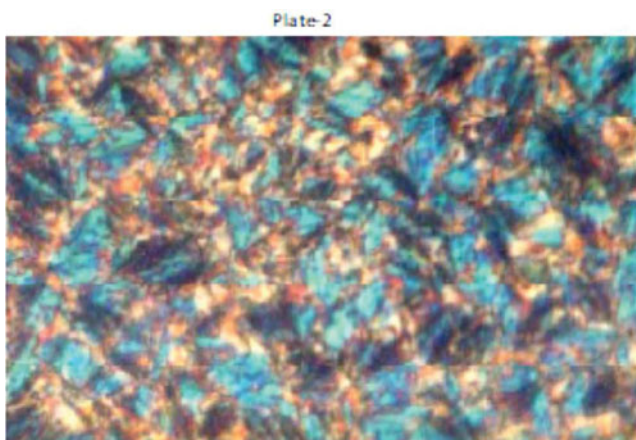


**Plate 2.** Broken focal conic fan texture of SmC phase for SA:11OBA at  $103^\circ\text{C}$ .

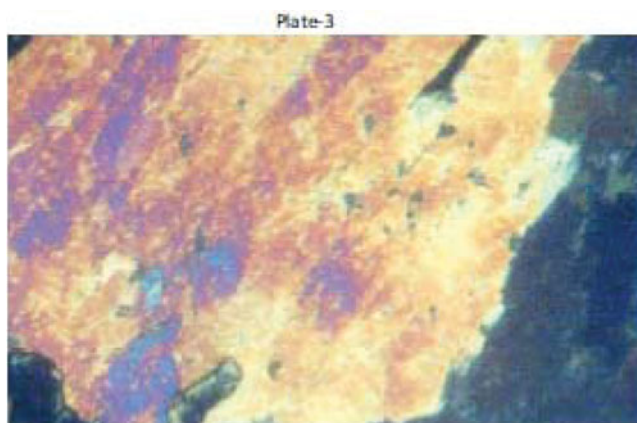


**Plate 3.** Colored mosaic texture of SmG phase exhibited by SA:11OBA at 85°C.

**Table 1.** Data of LC phases and transition temperatures.

HBLC	Method		Phase variance
11OBA	TM	Heating	Sld $\rightarrow$ (105.2) $\rightarrow$ SmC $\rightarrow$ (135.5) $\rightarrow$ N $\rightarrow$ (142.3) $\rightarrow$ Iso.
		Cooling	Iso $\rightarrow$ (135.1) $\rightarrow$ N $\rightarrow$ (124.5) $\rightarrow$ SmC $\rightarrow$ (83.5) $\rightarrow$ Sld.
	DSC	Heating	Sld $\rightarrow$ (105.24) $\rightarrow$ SmC $\rightarrow$ (135.51) $\rightarrow$ N $\rightarrow$ (142.36) $\rightarrow$ Iso. [117.05] [6.79] [8.11]
		Cooling	Iso $\rightarrow$ (135.16) $\rightarrow$ N $\rightarrow$ (124.48) $\rightarrow$ SmC $\rightarrow$ (83.4) $\rightarrow$ Sld. [8.32] [5.72] [31.36]
SA:11OBA	TM	Heating	Sld $\rightarrow$ (72.8) $\rightarrow$ SmG $\rightarrow$ (85.2) $\rightarrow$ SmC $\rightarrow$ (125.9) $\rightarrow$ N $\rightarrow$ (127.2) $\rightarrow$ Iso.
		Cooling	Iso $\rightarrow$ (127.2) $\rightarrow$ N $\rightarrow$ (125.9) $\rightarrow$ SmC $\rightarrow$ (85.2) $\rightarrow$ SmG $\rightarrow$ (72.8) $\rightarrow$ Sld.
	DSC	Heating	Sld $\rightarrow$ (97.6) $\rightarrow$ SmG $\rightarrow$ (128.2) $\rightarrow$ SmC $\rightarrow$ (129.6) $\rightarrow$ Iso. [97.4] [0.16] [0.97]
		Cooling	Iso $\rightarrow$ (127.2) $\rightarrow$ N $\rightarrow$ (125.9) $\rightarrow$ SmC $\rightarrow$ (85.2) $\rightarrow$ SmG $\rightarrow$ (72.8) $\rightarrow$ Sld. [0.67] [0.12] [26.03] [17.19]
	LF Dielectrics	Cooling	Iso $\rightarrow$ (127.1) $\rightarrow$ N $\rightarrow$ (126.0) $\rightarrow$ SmC $\rightarrow$ (85.0) $\rightarrow$ SmG $\rightarrow$ (72.7) $\rightarrow$ Sld.

Values in square brackets indicate enthalpy values ( $\Delta H$ ) in J.gm<sup>-1</sup>.

the broken focal conic fan texture, and SmG phase exhibits (Plate 3) the mosaic texture. The data of transition temperatures ( $T_C$ ) determined by POM are presented in Table 1. All LC phases exhibited by SA:11OBA are found to be enantiotropic.

### 3.4. Differential scanning calorimetry (DSC)

Differential scanning calorimetry thermograms recorded for SA:11OBA (at a rate of 10°C min<sup>-1</sup>) are presented in Fig. 4, and the data of transition temperatures ( $T_C$ ) and enthalpy ( $\Delta H$ ) are presented in Table 1. DSC data are found to agree with POM. Owing to the involvement of finite  $\Delta H$ , the I–N, N–SmC, SmC–SmG, and SmG–solid transitions are found to be of the first order nature.

### 3.5. Dielectric study of SA:11OBA complex

SA:11OBA is filled in 5- $\mu$ m spaced Device Tech (USA made polymer buffed, conductive coated) transparent glass cells when SA:11OBA is in its high temperature isotropic liquid state. Capacitance ( $\sim$ 48.87 pF) exhibited by empty cell is found to be invariant (Fig. 5) with temperature (30–100°C) and frequency (Fig. 6) in the range of RT (20 Hz–10 MHz) of interest. The



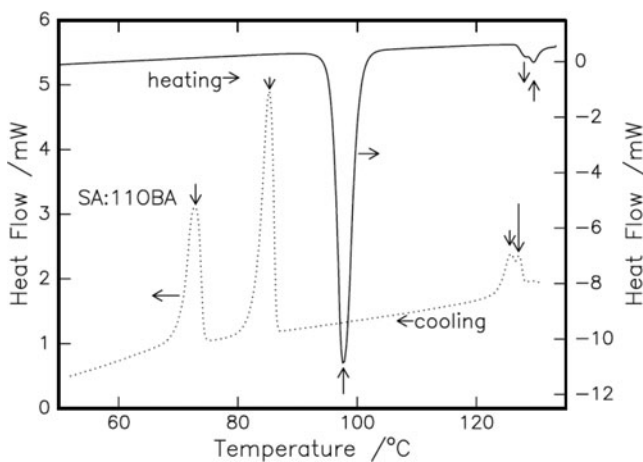


**Figure 4.** DSC thermogram for SA:110BA.

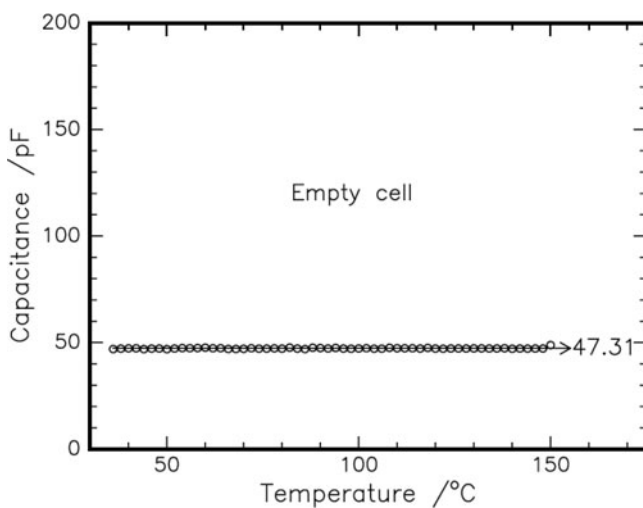


**Figure 5.** Temperature variation of capacitance  $C(T)$  exhibited by an empty cell.

temperature of the LC-filled cell is controlled by an Instec HCS-402 heating stage in conjunction with an STC-200 temperature controller. The leads connected to the cells are conveyed to the impedance analyzer. A Wayne Kerr 6500B (USA) Impedance analyzer is used to record dielectric dispersion in the low frequency (LF) range of 20 Hz to 10 MHz. Since LC-filled cell is placed on the microscope (POM) heating stage (set in crossed polar configuration), the data of capacitance  $C$  and loss factor  $\tan\Delta$  acquired can be simultaneously checked. The observations of optical textures (Plates 1–3) are used to confirm whether the dielectric data acquired at different temperatures pertain to the targeted LC phase of interest.

The observed temperature (Fig. 5) and frequency (Fig. 6) invariance of capacitance and loss factor, viz.  $C(T)$  and  $\tan\Delta(T)$  and  $C(\omega)$  and  $\tan\Delta(\omega)$ , by the empty cell reflect upon the absence of response from conductive coating (of the cells) or/and impurities (in the sample) in the temperature range of 25–155°C and the frequency range of 20 Hz to 10 MHz interest.

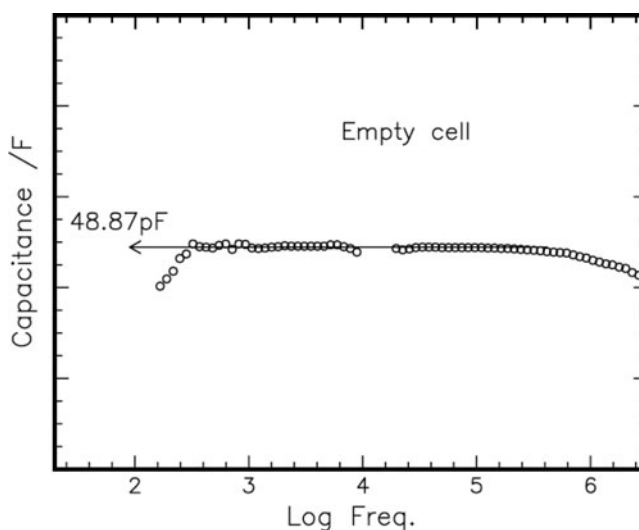


**Figure 6.** Frequency variation of capacitance  $C(\omega)$  and loss factor  $\tan\Delta(\omega)$  exhibited by an empty cell.

### 3.6. Phase transitions by LF dielectric measurements

Empty cell is heated in the vicinity of  $5^\circ\text{C}$  above the clearing temperature ( $\sim 145^\circ\text{C}$ ) of SA:11OBA isotropic temperature. A small speck of HBLC is introduced in the cell so that a thin sheet of LC spreads in the cell by capillary action. Since the temperature is far above the isotropic temperature of SA:11OBA, the LC in isotropic liquid phase comfortably enters the dielectric cell as a thin layer due to capillary action. Care is administered as to eliminate any small bubbles in the dielectric cell filled with the sample. The dielectric cell filled with LC sample is slowly cooled to room temperature and placed inside the Instec heating microscopic stage. SA:11OBA-filled dielectric cell is connected to impedance analyzer. Impedance analyzer is operated at 100 kHz (corresponding to 1  $V_{p-p}$  ac signal under bias-off configuration). Capacitance  $C$  and loss factor  $\tan\Delta$  are read from panels 1 and 2 of impedance analyzer. The temperature controller is programmed to reach  $5^\circ\text{C}$  above the reported [45] clearing temperature ( $\sim 45^\circ\text{C}$ ) of SA:11OBA. It is held there for 10 min and programmed to cool at a low rate of  $0.05^\circ\text{C}$  per minute down to the isotropic to nematic phase transition temperature. Impedance analyzer is operated at 1  $V_{p-p}$  oscillating signal under bias-off condition. The readings of capacitance  $C$  and loss factor  $\tan\Delta$  are noted in the LCR-meter mode. The readings of capacitance  $C(T)$  and loss factor  $\tan\Delta$  at different temperatures of interest are recorded in all LC phases exhibited by SA:11OBA with the decreasing temperature at 100-kHz frequency. Simultaneous microscopic textural observations are held to ensure that the data acquired for  $C(T)$  and  $\tan\Delta(T)$  pertain to the LC phases of interest exhibited by SA:11OBA. Variations in capacitance  $C(T)$  and loss factor  $\tan\Delta(T)$  exhibited by SA:11OBA cell with decreasing temperature  $C(T)$  are recorded in cooling scans. The observed variations in capacitance  $C(T)$  and loss factor  $\tan\Delta(T)$  exhibited by SA:11OBA cell are presented in Fig. 7. Peaks of temperature ( $T$ ) that are observed in capacitance  $C(T)$ , and dips observed in  $\tan\Delta$  are identified as phase transition temperatures. The phase transition temperatures, viz. I–N, N–SmC, SmC–SmG, and SmG–solid determined from LF dielectric studies are found to agree (Table 1) with the earlier observations [45] of POM and DSC. An overall decreasing trend of capacitance reflects upon the HBLC compounds entering a relatively condensed phase with lesser surface area. Increase of capacitance (in the vicinity of LC phase transition when it is entering into

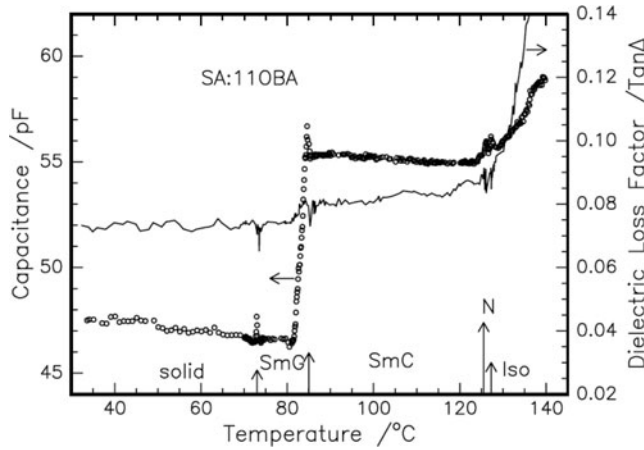


**Figure 7.** Temperature variation of capacitance  $C(T)$  and loss factor  $\tan\Delta(T)$  exhibited by SA:110BA cell.

a relatively ordered phase) with decreasing temperatures infers the increasing dipolar correlation across the LC phase transition. However, the capacitance  $C$  and the loss factor  $\tan\Delta$  are observed to remain almost invariant (or observed with a constant fall) with decreasing temperature in the equilibrium state of all LC phases exhibited by SA:110BA. The transition temperatures as recorded by LF dielectric studies (Table 1) are found to agree with the data determined by POM and DSC.

### 3.7. LF relaxation behavior

The variations of capacitance  $C(\omega)$  and loss factor  $\tan\Delta(\omega)$  are recorded at different specified temperatures in N, SmC, and SmG LC phases exhibited by SA:110BA.

The relative permittivity,  $\varepsilon_r$  (or  $\varepsilon'$ ) is estimated from

$$\varepsilon'(\omega) = \varepsilon_r(\omega) = [C_{\text{obs}}(\omega)]/48.87. \quad (1)$$

The dielectric loss  $\varepsilon''$  is estimated by

$$\varepsilon''(\omega) = \tan\Delta \times \varepsilon_r, \quad (2)$$

where  $\varepsilon_r$  is the relative permittivity of SA:110BA, i.e. the capacitance normalized over the capacitance exhibited (48.87 pF) by the empty cell.

The observed variation of loss  $\varepsilon''(\omega)$  in nematic phase with frequency recorded at different temperatures is found to exhibit two peaks in the LC phases of interest. The observed loss  $\varepsilon''$  with frequency  $\omega$  in nematic phase (as representative) is presented in Figs. 8 and 9 for LF (kHz) and HF (MHz) regions, respectively. Hence, the observed dispersion in SA:110BA is identified to exhibit two relaxation modes. The data of temperature variation of frequency  $f_R$ ,  $\varepsilon''_{\text{max}}$ , in LC phases are presented in Table 2. The frequency at which  $\varepsilon''$  exhibits a peak ( $\varepsilon''_{\text{max}}$ ) is identified as relaxation frequency  $f_R$  in both lower frequency (LF~kHz) and higher frequency (HF~MHz) relaxations. Both LF and HF relevant  $f_R$  values are observed to shift with temperature in all LC phases. A meticulous observation of  $\varepsilon''(\omega)$  about its peak value, i.e.  $\varepsilon''_{\text{max}}$  in all LC phases, reveals that the dielectric loss ( $\varepsilon''$ ) spreads about its maximum value ( $\varepsilon''_{\text{max}}$ ) rather non-symmetrically. Hence, the observed dispersion in N, SmC, and SmG LC phases [10–12] is considered to be off-centered. This off-centered [10–12] nature of dispersion

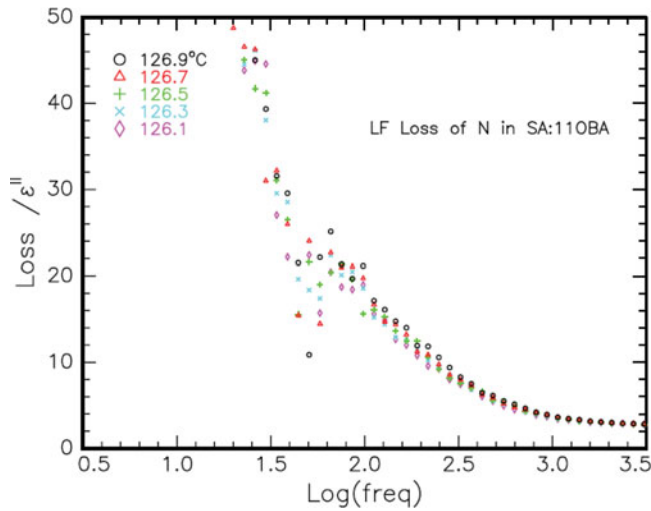


**Figure 8.** Frequency variation of dielectric loss  $\varepsilon''$  in N phase in kHz region.

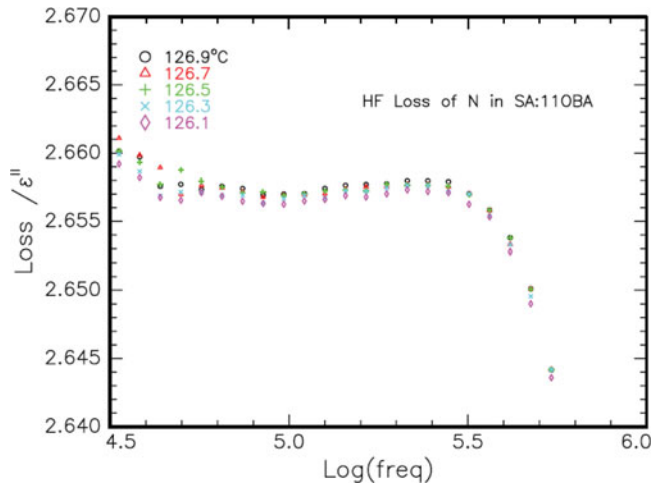


**Figure 9.** Frequency variation of loss  $\varepsilon''$  in N phase in MHz range.

infers a non-Debye-type of reorientation mechanism in LC phases exhibited by SA:110BA. Hence, the LF dielectric dispersion, viz.  $\varepsilon''(\omega)$  and  $\varepsilon_r(\omega)$ , observed at different temperatures in N, SmC, and SmG phases exhibited by SA:110BA is addressed [6, 10–12] through the relation

$$\varepsilon^*(\omega) = \varepsilon_\infty - \{(\varepsilon_o - \varepsilon_\infty)/[1 + j(\omega T)^{(1+\alpha)}]\}, \quad (3)$$

where,  $\varepsilon^*(\omega)$  is the complex permittivity,  $\varepsilon_\infty$  is the extrapolated high-frequency relative permittivity on  $\varepsilon_r$  axis in the Cole–Cole plots,  $\varepsilon_o$  is the extrapolated low-frequency relative permittivity on  $\varepsilon_r$  axis in the Cole–Cole plots,  $\alpha$  is the distribution parameter,  $j = \sqrt{-1}$ , and  $T$  is relaxation time given by  $[1/f_R]$ .

The off-centered dielectric dispersion, i.e.  $\varepsilon''(\omega)$  and  $\varepsilon_r(\omega)$ , recorded in N, SmC, and SmG phases is represented through the corresponding Cole–Cole plots in Fig. 10.

Owing to the fact that the present case of SA:110BA HBLC complex belongs to calamitic-type, the observed dispersion is expected to be off-centered non-Debye-type. Further, the dispersion is viewed as a response of a molecule of cylindrical shape [46] possessing finite

Table 2. Data of LF dielectric parameters  $f_R$  (T),  $\varepsilon''_{\max}$ ,  $\Delta\varepsilon$ ,  $\alpha$ , and activation energy  $E_d$  in N, SmC, and SmG phases of SA:110BA.

Phase variance	Temperature (°C)	Low-frequency relaxation				High-frequency relaxation			
		$f_R$ (kHz)	$\varepsilon''_{\max}$	$\Delta\varepsilon = [\varepsilon_0 - \varepsilon_\infty]$	$\alpha$	$f_R$ (MHz)	$\varepsilon''_{\max}$	$\Delta\varepsilon = [\varepsilon_0 - \varepsilon_\infty]$	$\alpha$
N [0.473] [3.629]	126.7	1.8174	2.6730	19.10	0.20952	5.3315	19.14	1.91	0.06984
	126.5	1.8479	2.6673	19.20	0.24444	5.3478	18.66	1.90	0.05238
	126.3	1.8712	2.6576	19.80	0.31428	5.3511	17.94	1.84	0.03492
	126.1	1.9913	2.6573	20.70	0.38412	5.4717	17.10	1.76	0.01746
SmC {0.301} [0.102]	125.8	1.7602	26.279	47	0.2619	5.3880	2.6571	2.09	0.08730
	123.8	1.7670	20.00	33.2	0.2270	5.3895	2.6560	2.08	0.06984
	121.8	1.8201	16.20	25.3	0.1921	5.4086	2.6652	2.03	0.05238
	115.8	1.8738	13.442	21.4	0.1746	5.4243	2.6532	2.01	0.03472
SmG {0.109} [0.137]	115.4	1.9940	4.164	5.7	0.1222	5.4451	2.6528	1.94	0.01746
	84.5	1.3586	11.401	10.8	0.0698	5.3586	2.6522	1.87	0.01746
	80.0	1.3847	8.412	9.1	0.1048	5.3885	2.6572	1.88	0.02619
	78.0	1.4173	6.620	7.7	0.1397	5.4212	2.6545	1.89	0.03050
	74.0	1.5315	5.737	5.8	0.1746	5.4456	2.6551	1.90	0.03492

Data in {} denotes LF activation energy in eV; and data in [] denote HF activation energy in eV

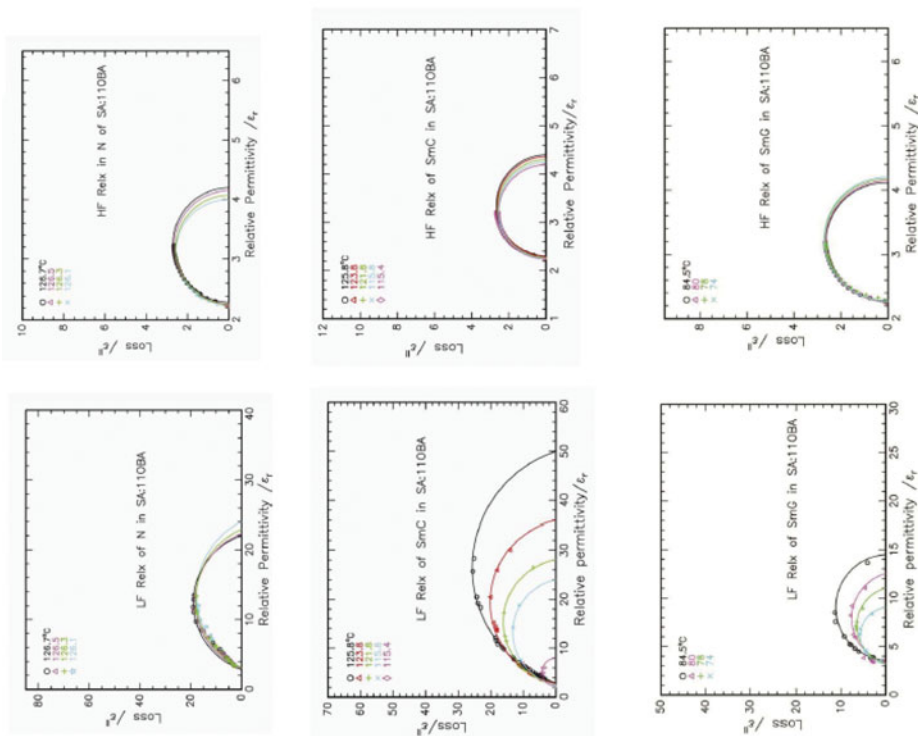


**Figure 10.** Cole–Cole plots in N, SmC, and SmG phases exhibited by SA:110BA.

length to breadth ratio. The dielectric permittivity ( $\epsilon'$  or  $\epsilon_r$ ) loss exhibited by SA:110BA in any LC phase at a finite temperature is found to decrease with increasing frequency, although it exhibits two non-symmetrical loss ( $\epsilon''$ ) peaks, viz. one in LF (kHz) region and the other in HF (MHz) region. The two peaks infer two types of reorientation mechanisms of molecular dipoles to the field. Further, the investigations are carried out to understand these LF and HF relaxation processes by drawing the Cole–Cole plots (Fig. 9) in N, SmC, and SmG phases exhibited by SA:110BA.

The frequency at which loss ( $\epsilon''$ ) exhibits a peak is considered as the relaxation frequency  $f_R$  (whose reciprocal stands for the relaxation time  $\tau_R$ ). The observed loss spectrum (Figs. 8 and 9) viewed against that exhibited by the empty cell (Figs. 5 and 6) confirms that peaks in  $\epsilon''$  are the contribution of LC materials. The  $\epsilon''_{\max}$  values in any phase are found to shift with



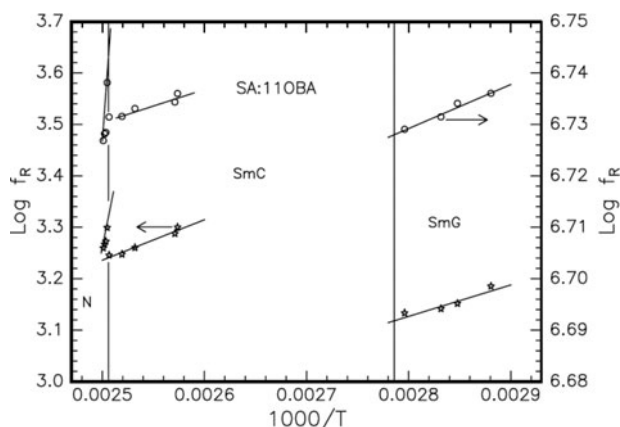


**Figure 11.** Arrhenius plots in N, SmC, and SmG phases of SA:11OBA.

decreasing temperatures to reveal the underlying Arrhenius shift. The observed temperature shift in  $f_R$ , loss maximum  $\varepsilon''_{\max}$ , dielectric strength  $\Delta\varepsilon$  ( $\varepsilon_0 - \varepsilon_\infty$ ) (estimated from the Cole–Cole plots), and the distribution parameter ( $\alpha$ ) for both relaxation modes in N, SmC, and SmG phases are presented in Table 2. The observed (Arrhenius shift) of  $f_R$  studied in all the LC phases exhibited by SA:11OBA are presented in Fig. 11. Activation energies ( $E_a$ ) estimated from the Arrhenius plots in N, SmC, and SmG phases are presented in Table 2. These are found to agree with the range of activation energies reported [50–52] in other calamitic LCs in their N, SmC, and SmG phases. The activation energy observed in SA:11OBA for both lower and higher frequency relaxation mechanisms are also found to be slightly less than the values reported [50–52] in smectic phases exhibited by other calamitic LCs without hydrogen bonding interaction on their molecular body. HB interaction is argued to lessen the activation energy in smectic phases during their reorientation process to the applied field.

### 3.8. Reorientation mechanism

An overview of molecular structure (Scheme 1) suggests that in the case of SA:11OBA, the rigid core is made of two aromatic cores of nOBA moieties. The rigid core also contains the HB interaction region. The rigid core is attached laterally to long flexible end chains ( $-\text{C}_n\text{H}_{2n+1}$ ) through an electro negative oxygen atom on both sides. Hence, the longitudinal dipole moment  $\mu_1$  is expected to extend through the rigid core part and on the oxygen atom. However,  $\mu_1$  entails over the flexible end chains also. Since  $\mu_1$  centered at O-atom configures in relatively rigid part of molecular frame, it is expected to respond faster than that of  $\mu_1$  spread over flexible end chains. Therefore, the HF relaxation process is related to the reorientation of  $\mu_1$  located at the bridging of O-atom, while LF process is attributed to the reorientation of  $\mu_1$  situated on the flexible part of the molecule. The present case of varied time scale relaxation behavior is found [49] to be analogous to that observed in multiple relaxations in other calamitic LCs that do not possess HB interaction on their molecular frame.

It is noted that the relaxation frequency  $f_R$ , the dielectric strength  $\Delta\varepsilon$ , and the distribution parameter  $\alpha$  (reflecting the degrees of freedom experienced by molecular dipole during its reorientation of applied field) are found (Table 2) to follow characteristic trends with decreasing temperature in all LC phases. Shift in dielectric parameters, viz.  $f_R$ ,  $\varepsilon''_{\max}$ ,  $\Delta\varepsilon$ , and  $\alpha$ , is found to be relatively large in case of LF relaxations. The LF activation energy ( $E_a$ ) is

found to decrease as one goes from nematic phase to SmG phase. However, in the case of HF relaxations, reverse trend in  $E_a$  is observed as one goes from SmC to SmG phase. It is also noted that the loss maximum  $\varepsilon''_{\max}$  is accompanied with a decrease in almost all LC phases (except for HF relaxation in SmG). The magnitude of dielectric strength  $\Delta\varepsilon$  exhibited for LF mode seems to be higher than that exhibited for HF relaxation. Higher  $\Delta\varepsilon$  suggests a relatively large range of LF operation for the mode of vibration with a sluggish response of  $\sim 1$  ms.

## 4. Conclusions

- LF dielectric investigations in HBLCs are useful to determine phase transition temperatures  $T_C$  and thermal stability  $\Delta T$ .
- Any small structural change due to change in dipolar correlation can be effectively studied by LF dielectric method than that with DSC.
- HBLC complexes of SA:11OBA-type comprising rigid core and flexible parts of molecular body exhibit two distinct modes of relaxation behavior.
- LF (kHz) mode of relaxation exhibits long range of operation and large absorption in HBLCs.
- Activation energies estimated in N, SmC, and SmG phases exhibited by HBLCs of SA:11OBA-type agree with that of other non-HB calamitic LCs.

## Funding

The authors acknowledge the financial support (DST/SR/S2/CMP-0063/2008) from the Department of Science and Technology, Ministry of Science & Technology, Govt. of India, New Delhi, India.

## References

- [1] Luckhurst, G. W. (1979). *Gray in the Molecular Physics of Liquid Crystals*, Academic Press: New York, NY.
- [2] Meier, G., Sackmann, E., & Grabmaier, J. G. (1975). *Applications of Liquid Crystals*, Springer-Verlag: Berlin, Germany.
- [3] Blinov, L. M., & Chigrinov, V. G. (1994). *Electro-Optic Effects in LC Materials*, Springer-Verlag: New York, NY.
- [4] Brock, J. D., Birgeneau, R. J., Litster, J. D., & Aharony, A. (1989, July). *Phys. Today*, 42, 52–59.
- [5] de Gennes, P. G. (1975). In: *The Physics of Liquid Crystals*, Chpt. 5, pp. 153–210, Eds. W. Marshall and D. H. Wilkinson, Clarendon Press: Oxford, UK.
- [6] Hills, N. E., Wanghan, W. E., Price, A. H., & Davies, M. (1969). In: *Dielectric Properties and Molecular Behaviour*, Ch. 1, pp. 1–106, von Nostrand (Ed.), New York, NY.
- [7] Anderson, G., Dhal, J., Kuczinski, W., Lagerwall, S. T., Skarp, K., & Stebler, B. (1988). *Ferroelectrics*, 84, 285–315.
- [8] Gouda, F., Skarp, K., & Lagerwall, S. T. (1991). *Ferroelectrics*, 113, 165–206.
- [9] Gouda, F., Skarp, K., Lagerwall, S. T., Escher, C., & Kresse, W. H. (1991). *J. de Phys.*, 11, 167–188.
- [10] Cole, R. H., & Davidson, D. W. (1952). *J. Chem. Phys.*, 20, 1389–1397.
- [11] Cole, R. H. (1957). *J. Chem. Phys.*, 27, 33–38.
- [12] Kresse, H., & Moscicki, J. K. (1980). In: *Advances in Liquid Crystal Research and Applications*, Proceedings of the 3rd LC Conference, Molecular Dynamics and Dynamical Methods: A dielectric study of nematogen 4-n-hexyloxyphenyl 4-n-methoxybenzoate, C10/OC6, pp. 287–296, Budapest, Pergamon Press: Oxford, UK.

- [13] Demus, D. (1976). In: *Non-Emissive Electro-Optic Displays*, Session 3: Chemical Composition and Display Performance, pp. 83–117, Eds. A. R. Kmetz and F. K. Von Willisen, Plenum Press: New York, NY.
- [14] Goodby, J. W., Blink, R., Clark, N. A., Lagerwall, S. T., Osipov, S. A., Pikin, S. A., *et al.* (1991). In: *Ferro-Electric Liquid Crystal, Principles, Properties and Applications*, Gordon and Breech Press: Philadelphia, PA.
- [15] Paleos, C. M., & Tsiourvas, D. (1995). *Angew. Chem. Int. Ed. Engl.*, **34**, 1696–1711.
- [16] Paleos, C. M., & Tsiourvas, D. (2001). *Liq. Cryst.*, **28**, 1127–1161.
- [17] Kato, T., & Fréchet, J. M. J. (1989). *J. Am. Chem. Soc.*, **111**, 8533–8534.
- [18] Kato, T., Wilson, P. G., Fujishima, A., & Fréchet, J. M. J. (1990). *Chem. Lett.*, **19**, 2003–2006.
- [19] Fukusama, M., Kato, T., Uryu, T., & Fréchet, J. M. J. (1993). *Chem. Lett.*, **22**, 65–68.
- [20] Kato, T., Fréchet, J. M. J., Wilson, P. G., Saito, T., Uryu, T., Fujishima, U., *et al.* (1993), *Chem. Mater.*, **5**, 1094–1100.
- [21] Kato, T., Fukumasa, M., & Fréchet, J. M. J. (1995). *Chem. Mater.*, **7**, 368–372.
- [22] Kahira, H., Kato, T., Uryu, T., Ujiie, S., Kumar, U., Fréchet, J. M. J., *et al.* (1996). *Liq. Cryst.*, **21**, 25–30.
- [23] Gray, G. W., & Jones, B. J. (1953). *J. Chem. Soc.*, **4**, 4179–4180.
- [24] Kato, T., Mizoshita, N., & Kishimoto, K. (2006). *Angew Chem. Intl.*, **45**, 38–68.
- [25] Srinivasulu, M., Satyanarayana, P. V. V., Kumar, P. A., & Pisipati, V. G. K. M. (2001). *Liq. Cryst.*, **28**, 1321–1329.
- [26] Kato, T., Fréchet, J. M. J., Uryu, T., Kaneuchi, F., & Jin, C. (2006). *Liq. Cryst.*, **33**, 1429–1437.
- [27] Lavigueur, E. J., Foster, E. J., & Williams, V. E. (2008). *J. Am. Chem. Soc.*, **130**, 11791–11800.
- [28] Swathi, P., Kumar, P. A., & Pisipati, V. G. K. M. (2000). *Liq. Cryst.*, **27**, 665–669.
- [29] Kumar, P. A., Srinivasulu, M., & Pisipati, V. G. K. M. (1999). *Liq. Cryst.*, **26**, 1339–1343.
- [30] Swathi, P., Kumar, P. A., & Pisipati, M. (2001). *Z.Naturf.*, **56a**, 692–696.
- [31] Kumar, P. A., Pisipati, V. G. K. M., Rajeswari, A. V., & Sastry, S. S. S. (2002). *Z. Naturf.*, **57a**, 184–188.
- [32] Attla, K., Andere, S., & Istvan, H. (2002). *Acc. Chem. Res.*, **35**, 887–894.
- [33] Armstrong, G., & Buggy, M. (2005). *J. Mater. Sci.*, **40**, 547–559.
- [34] Katranchev, B., Naradikian, H., & Petrov, M. (2005). *J. Opt. Eelectr. Adv. Mater.*, **7**, 273–276.
- [35] Fréchet, J. M. J., & Kato, T. (1992). US Patent No. 5139696.
- [36] Tian, Y., Xu, X., Zhao, Y., Tang, X., Li, T., Sun, J., *et al.* (1996). *Thin Solid Film*, **284**, 603–605.
- [37] Bhat, S. G., Srinivasulu, M., Girish, S. R., Padmalatha, R., Bhagavath, P., Maha Baleshwara, S., Muniprasad, M., & Potukuchi, D. M. (2012). *Mol. Cryst. Liq. Cryst.*, **552**, 83–96.
- [38] Meier, W., & Meier, G. (1961). *Z. Naturf.*, **16a**, 470–477.
- [39] Meier, G., & Saupe, A. (1966). *Mol. Cryst.*, **1**, 515–525.
- [40] Rondalez, F., Diguët, D., & Durand, G. (1971). *Mol. Cryst. Liq. Cryst.*, **15**, 183–188.
- [41] Agarwal, V. K., & Price, A. H. (1974). *J. Chem. Soc. Faraday Trans.*, **2**, 188–192.
- [42] Kresse, H., Schmidt, P., & Demus, D. (1975). *Phys. Stat. Solid (a)*, **32**, 315–320.
- [43] Sreedevi, B., Chalapathi, P. V., Kotikalapudi, V. K. M., Pisipati, V. G. K. M., & Potukuchi, D. M. (2007). *Ferroelectrics*, **361**, 18–36.
- [44] Muniprasad, M., Srinivasulu, M., Chalapathi, P. V., & Potukuchi, D. M. (2012). *J. Mol. Struct.*, **1015**, 181–191.
- [45] Muniprasad, M. (2012). In: *Synthesis and Characterization of Supra-Molecular Liquid Crystals*, Ph.D. Thesis, Ch. 3, 187–214, Jawaharlal Nehru Technological University Kakinada, India.
- [46] Priestley, E. B., Wojtowicz, P. J., & Sheng, P. (1975). In: *Introduction to Liquid Crystals*, Ch. 2, 15–27, Ed. Aaron W. Levine, Plenum Press, New York.
- [47] Silverstein, R. M., & Webster, F. X. (2004). In: *Spectroscopic Identification of Organic Compounds*, Ch. 3, 80–108 & Ch. 4, 151–204, 7th Ed., John Wiley: New Jersey.
- [48] William, K. (2008). In: *Organic Spectroscopy*, Ch. 2 & 3, 19–171, Replika Press: India.
- [49] Gray, G. W., & Goodby, J. W. (1984). In: *Smectic Liquid Crystal Textures and Structures*, Ch. 3, 45–64 & Ch. 7, 105–116, Leonard Hill: London.
- [50] Potukuchi, D. M., & George, A. K. (2008). *Mol. Cryst. Liq. Cryst.*, **487**, 92–109.
- [51] Rani, G. P., Potukuchi, D. M., & Pisipati, V. G. K. M. (1998). *Liq. Cryst.*, **25**, 589–595.
- [52] Rani, G. P., Potukuchi, D. M., Rao, N. V. S., & Pisipati, V. G. K. M. (1994). *Solid State Commn.*, **92**, 349–352.